UNIVERSITY OF BATH

Link to publication

University of Bath

Surface-induced nonlinearity enhancement in subwavelength rod waveguides

A. Marini, R. Hartley, A. V. Gorbach, and D. V. Skryabin

Centre for Photonics and Photonic Materials, Department of Physics, University of Bath, Bath BA2 7AY, United Kingdom

We develop a perturbative theory to describe optical propagation in subwavelength rod waveguides. In this approach, we account for loss and nonlinearity in the boundary conditions. A comparison to the traditional perturbative approach used in optical fibers reveals that the surface contribution provides a significant nonlinearity enhancement in the subwavelength regime. We further compare the nonlinearity enhancement of metallic, dielectric, and semiconductor waveguides, in addition to determining the attenuation coefficient of metallic nanowires.

I. INTRODUCTION

Light guidance and manipulation at the subwavelength scale has become the subject of intense research in recent years. It is driven by a substantial improvement of nanofabrication techniques and the need for compact high performance optical devices. Among the promising candidates for light guidance at the nanometer scale are plasmonic waveguides [1,2]. Their operation relies on the excitation of surface plasmon polaritons (SPP) at metal-dielectric interfaces [3]. Dielectric and semiconductor nanowires, where light guidance in a subwavelength-sized core is achieved due to a high refractive index contrast, is another competing platform [4–7].

A common theoretical approach to describe the different nonlinear processes in waveguides and fibers is based on a nonlinear Schödinger-type equation for the slowly varying amplitude of a guided mode, which is derived by perturbation expansions assuming weak nonlinearities and losses (see, e.g., Ref. [8]). In this approach, the transverse field profile is assumed to be fixed by the waveguide geometry and is found in the lowest order of the perturbation expansion as a solution of the corresponding linear Maxwell equations. Nonlinear polarization and possible losses are accounted for in the higher orders and result in a slow variation in propagation distance of the mode amplitude. We emphasize that corrections to boundary conditions at the waveguide interface due to nonlinearity and loss are usually disregarded. This is justified for large-core waveguides, where field intensities are typically weak at the waveguide interface. However, in subwavelength geometries, particularly in plasmonic waveguides where the field intensity peaks at the interfaces [3], this is generally not true and the validity of the approach becomes questionable [9].

As we previously illustrated by considering simple planar geometries [9], the rigorous account for the above corrections to the boundary conditions leads to a significant surface-induced enhancement of the nonlinear and loss coefficients in the resulting propagation equation. Our theory confirms previously reported experimental and theoretical findings [5–7,10], while offering a more transparent and rigorous approach and provides physical insight into the effects of nonlinearity enhancement in nanoscaled geometries. In this work, we extend our approach to the case of rod waveguides and illustrate nonlinearity enhancement for different metallic, and dielectric or semiconductor setups.

The general idea of our approach is sketched in Sec. II. In Sec. III we consider dispersion of linear guided modes in rod waveguides. The propagation equation which describes evolution of slowly varying amplitude of a guided mode is derived in Sec. IV. The main result of our work is incorporated in the unique surface-induced enhancement factor g, Eq. (28), which summarizes the impact of field discontinuities at the waveguide interface on the effective nonlinear coefficient of the structure. Finally, in Sec. V, we apply our theory for analysis of the nonlinearity enhancement in different waveguides and identify resonant mechanisms behind this enhancement.

II. PERTURBATION EXPANSION

We start from the dimensionless, time-independent Maxwell equations,

$$\vec{\nabla} \times \vec{E} = ic\mu_0 \vec{H}, \tag{1}$$

$$\vec{\nabla} \times \vec{H} = -ic\epsilon_0(\epsilon_a + i\epsilon_b)\vec{E} - ic\vec{D}_{nl}, \tag{2}$$

where the spatial coordinates are scaled by $k = \omega/c$, with ω as the field angular frequency and c the speed of light. We choose to work in cylindrical coordinates (ρ, ϕ, z), where the rod waveguide geometry is given by the real-valued dielectric susceptibility function $\epsilon_a(\rho) = \epsilon_I \theta(r - \rho) + \epsilon_O \theta(\rho - r)$. Here $r = Rk$, R is the core radius, $\theta(x)$ is the Heaviside step function, and ϵ_I, ϵ_O are the dielectric constants of the core and cladding materials, respectively. $\epsilon_b(\rho)$ accounts for losses, while $\vec{D}_{nl}$ is the nonlinear contribution to the displacement vector. For the case of isotropic Kerr nonlinearity, the latter is given by [10]

$$\vec{D}_{nl}(\vec{E}) = \frac{\epsilon_0 \chi_3(\rho)}{2}\left[|\vec{E}|^2\vec{E} + \frac{1}{2}\vec{E}^2\vec{E}^*\right]. \tag{3}$$

Below we assume that losses and nonlinearity have the same order of smallness $O(s^{3/2})$, where $s \ll 1$ is a dummy small parameter, $\epsilon_b/\epsilon_a \sim s$. To solve Eqs. (1) and (2) we use the following ansatz:

$$\vec{E} = [I^{1/2}\psi(z)\vec{e}(\rho) + \vec{j}(\rho,\phi,z) + O(s^{5/2})] \times e^{i\beta z + im\phi}, \tag{4}$$

$$\vec{H} = \epsilon_0 c[I^{1/2}\psi(z)\vec{h}(\rho) + \vec{l}(\rho,\phi,z) + O(s^{5/2})] \times e^{i\beta z + im\phi}, \tag{5}$$

where $\psi \sim s^{1/2}$, $\partial_z \psi \sim s\psi \ll \beta\psi$, $\vec{j}, \vec{l} \sim s^{3/2}$, $\vec{e} = (e_\rho, e_\phi, e_z)^T$, and $\vec{h} = (h_\rho, h_\phi, h_z)^T$ give the linear guided mode profile, β is the mode propagation constant, and $m \in \mathbb{Z}$ is the winding number. The above substitution also applies to the boundary conditions: continuity of the tangential components of the electric field and normal component of the displacement vector. Without loss of generality $\vec{e}$ and $\vec{h}$ can be assumed dimensionless, so that the field units are carried by $I^{1/2}\psi$. The normalization factor I is chosen below [see Eq. (16)] such that $|\psi|^2$ is the power (measured in watts) carried in the z direction.

Substituting this ansatz into Maxwell equations (1) and (2) and collecting terms of the order $O(s^{1/2})$ we obtain linear mode profiles and corresponding propagation constants, while terms of the order $O(s^{3/2})$ eventually give us the propagation equation for the function $\psi(z)$.

III. LINEAR GUIDED MODES

We express the transverse components of the fields $e_\rho, e_\phi, h_\rho, h_\phi$ in terms of the longitudinal ones e_z, h_z [11]:

$$e_\rho = -\frac{i}{q^2}[im(1/\rho)h_z + \beta\partial_\rho e_z], \quad (6)$$

$$e_\phi = \frac{i}{q^2}[\partial_\rho h_z - im\beta(1/\rho)e_z], \quad (7)$$

$$h_\rho = \frac{i}{q^2}[im\epsilon_a(1/\rho)e_z - \beta\partial_\rho h_z], \quad (8)$$

$$h_\phi = -\frac{i}{q^2}[\epsilon_a\partial_\rho e_z + im\beta(1/\rho)h_z], \quad (9)$$

where $q^2 = \beta^2 - \epsilon_a$. From Maxwell equations we obtain

$$e_z = A\frac{J_m(iq_I\rho)}{J_m(iq_Ir)}\theta(r-\rho) + C\frac{H_m(iq_O\rho)}{H_m(iq_Or)}\theta(\rho-r), \quad (10)$$

$$h_z = B\frac{J_m(iq_I\rho)}{J_m(iq_Ir)}\theta(r-\rho) + D\frac{H_m(iq_O\rho)}{H_m(iq_Or)}\theta(\rho-r), \quad (11)$$

where $q_{I,O} = \sqrt{\beta^2 - \epsilon_{I,O}}$, and J_m, H_m are the modified Bessel and Hankel functions of the mth order, respectively. Boundary conditions provide a homogeneous system of four algebraic equations for the constants A, B, C, D; the solution is nontrivial only if the determinant of the coefficient matrix is zero, which yields the dispersion relation [12],

$$\left[q_I\epsilon_O\frac{H'_m(iq_Or)}{H_m(iq_Or)} - q_O\epsilon_I\frac{J'_m(iq_Ir)}{J_m(iq_Ir)}\right]$$
$$\times \left[q_O\frac{J'_m(iq_Ir)}{J_m(iq_Ir)} - q_I\frac{H'_m(iq_Or)}{H_m(iq_Or)}\right] = \left[\frac{m\beta(\epsilon_O - \epsilon_I)}{q_Oq_Ir}\right]^2. \quad (12)$$

The prime of the functions denotes the derivative with respect to the argument of the functions J_m and H_m. The solution of this transcendental equation for any fixed m gives the mode propagation constant β, which is then used to calculate coefficients $A-D$ and restore the corresponding mode profile.

We note that the derived localized modes cut off when q_O becomes imaginary, and that modes with the same $|m|$ have equal propagation constants β.

For $m = 0$, the dispersion relation can be factorized as the product of two β functions. The roots of these functions provide transverse electric (TE; $e_z = e_\rho = 0, e_\phi \neq 0$) and transverse magnetic (TM; $h_z = h_\rho = 0, h_\phi \neq 0$) modes. For any $m > 0$ there are, generally, two types of modes (HE and EH modes) where all three electric field components are nonzero [11]. However, for metallic nanowires, only one mode exists at any fixed $|m|$ [13].

By calculating the z component of the Poynting vector for a particular guided mode,

$$P_z = (\pi/k^2)\int_0^{+\infty}\rho\text{Re}[E_\rho H_\phi^* - E_\phi H_\rho^*]d\rho$$
$$= \frac{\epsilon_0 c}{2k^2}\beta I|\psi|^2(1+\eta)P, \quad (13)$$

where

$$P = 2\pi\int_0^{+\infty}\rho|\vec{e}|^2d\rho, \quad (14)$$

$$\eta = \frac{2\pi r}{\beta P}\text{Im}[e_\rho^* e_z]_{r^-}^{r^+}, \quad (15)$$

we obtain the normalization factor:

$$I = 2k^2/[\beta\epsilon_0 c(1+\eta)P]. \quad (16)$$

Hereafter we use notation $[f(\rho)]_{r^-}^{r^+} = \lim_{\delta\to 0}[f(r+\delta) - f(r-\delta)]$. Note, that η is generally nonzero since e_ρ is discontinuous across the boundary.

IV. PROPAGATION EQUATION

Combining Eqs. (1) and (2) into the single equation for electric field, in the order $O(s^{3/2})$ of the perturbation expansion, we obtain

$$\hat{L}_m\vec{j} = I^{1/2}\left(i\epsilon_b\psi - \partial_z\psi\hat{D}_z^{(m)}\right)\vec{e} + \frac{1}{\epsilon_0}\vec{D}_{nl}(I^{1/2}\psi\vec{e}), \quad (17)$$

where

$$\hat{L}_m = \begin{pmatrix} q^2 + \frac{m^2}{\rho^2} & \frac{im}{\rho^2}\partial_\rho\rho & i\beta\partial_\rho \\ im\partial_\rho\frac{1}{\rho} & q^2 - \partial_\rho\frac{1}{\rho}\partial_\rho\rho & -\frac{m\beta}{\rho} \\ \frac{i\beta}{\rho}\partial_\rho\rho & -\frac{m\beta}{\rho} & p^2 - \partial_\rho\frac{1}{\rho}\partial_\rho\rho \end{pmatrix} \quad (18)$$

is the linear Maxwell operator in cylindrical coordinates, $p^2 = (m^2 - 1)/\rho^2 - \epsilon_a$, and

$$\hat{D}_z^{(m)} = \begin{pmatrix} -2i\beta & 0 & \partial_\rho \\ 0 & -2i\beta & \frac{im}{\rho} \\ \frac{1}{\rho}\partial_\rho\rho & \frac{im}{\rho} & 0 \end{pmatrix}. \quad (19)$$

The propagation equation can be determined by taking the scalar product of both sides of Eq. (17) with the linear mode $\vec{e}$:

$$\langle\vec{e}|\hat{L}_m|\vec{j}\rangle = -I^{1/2}\partial_z\psi\langle\vec{e}|\hat{D}_z^{(m)}|\vec{e}\rangle$$
$$+ iI^{1/2}\psi\langle\vec{e}|\epsilon_b|\vec{e}\rangle + \frac{1}{\epsilon_0}\langle\vec{e}|\vec{D}_{nl}\rangle. \quad (20)$$

If one neglects corrections in the boundary conditions (BCs) due to loss and nonlinearity [8,14], then $\langle\vec{e}|\hat{L}_m|\vec{j}\rangle = 0$, since $\vec{e}$ is the eigenvector of the self-adjoint operator $\hat{L}_m$ which has a zero eigenvalue. However, the corrections in the BCs remove
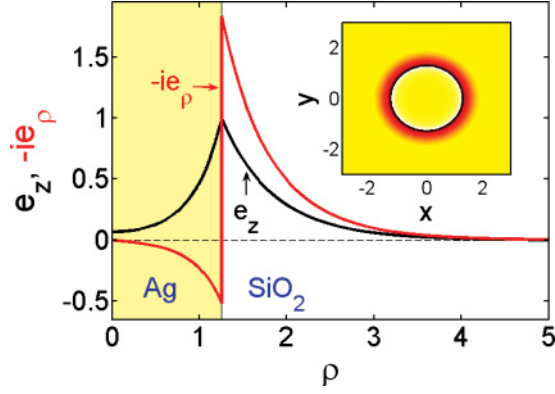
FIG. 1. (Color online) TM guided mode, $m = 0$, of silver rod waveguide with silica glass cladding, waveguide radius $R = 100$ nm, $\lambda = 500$ nm. Inset shows cross section of the z component of the Poynting vector, colors change from black corresponding to large positive values, through yellow (light gray) corresponding to zero and white corresponding to the smallest negative value (thin region in the metal core near the boundary).

the self-adjoint property in the order $O(s^{3/2})$: $\langle \vec{e}|\hat{L}_m|\vec{j}\rangle \neq \langle \vec{j}|\hat{L}_m|\vec{e}\rangle^* \neq 0$. The full set of BCs is

$$[E_z]_{r^-}^{r^+} = [H_z]_{r^-}^{r^+} = [E_\phi]_{r^-}^{r^+} = 0, \tag{21}$$

$$\left[(\epsilon_a + i\epsilon_b)E_\rho + \frac{1}{\epsilon_0}D_{nl,\rho}\right]_{r^-}^{r^+} = 0. \tag{22}$$

Performing the integral $\langle \vec{e}|\hat{L}_m|\vec{j}\rangle$, and applying the above BCs, where terms up to $O(s^{3/2})$ order are kept, we obtain

$$\langle \vec{e}|\hat{L}_m|\vec{j}\rangle = 2\pi r I^{1/2}\partial_z\psi[e_z^* e_\rho]_{r^-}^{r^+}. \tag{23}$$

Note that $\vec{e}$ satisfies the BCs (21), (22) in the order $O(s^{1/2})$, and therefore e_z and e_ϕ are continuous, while e_ρ is discontinuous at the waveguide interface $\rho = r$ (see Figs. 1, 4, and 7). As a result, the right-hand side of Eq. (23) is generally nonzero. The approximation $\langle \vec{e}|\hat{L}_m|\vec{j}\rangle \simeq 0$ is well satisfied for waveguides with a small index step and a large core radius $R \gg \lambda$ (such as, e.g., conventional optical fibers). Indeed, in this regime, the longitudinal component of the electric field is generally small, while discountinuity in e_ρ is proportional to $|\epsilon_I - \epsilon_O|$ and also small. However, for subwavelength waveguides with large refractive index contrasts and small core sizes, this approximation is no longer valid, and the surface term in Eq. (23) becomes essential [9].

Direct calculation of $\langle \vec{e}|\hat{D}_z^{(m)}|\vec{e}\rangle$ reveals another contribution from the surface:

$$\langle \vec{e}|\hat{D}_z^{(m)}|\vec{e}\rangle = -2i\beta P - 2\pi r[e_z e_\rho^*]_{r^-}^{r^+}, \tag{24}$$

where the quantity P is given by Eq. (14). At this point we would like to emphasize that the rigorous account of surface terms *from both sides* of Eq. (17) eventually leads to a *real-valued* nonlinearity enhancement factor g (see below). On the contrary, by ignoring the surface contribution in the left-hand side of Eq. (20) (i.e., by setting $\langle \vec{e}|\hat{L}_m|\vec{j}\rangle = 0$), one would generally obtain a nonphysical complex enhancement factor g for $m \neq 0$ modes. Also, as we illustrated previously [9], the rigorous account for all surface terms is necessary to obtain the correct diffraction coefficient in planar geometries.
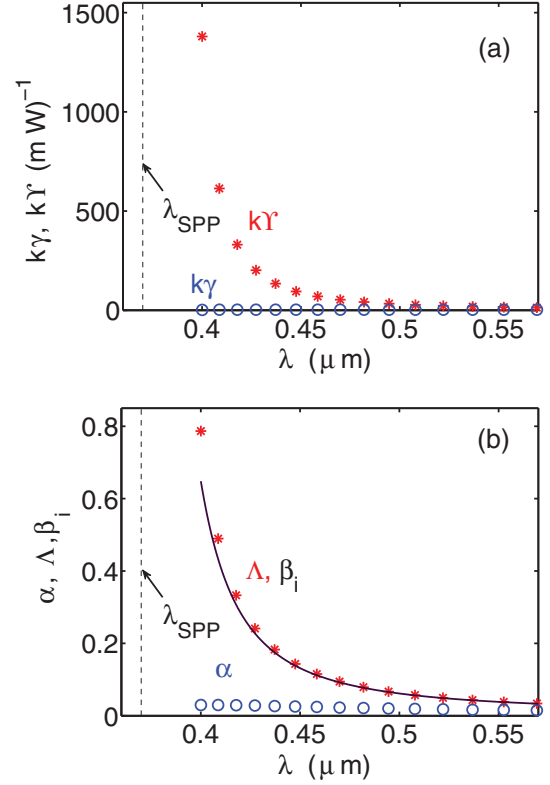

FIG. 2. (Color online) Nonlinear (a) and loss (b) coefficients of the silver waveguide mode as in Fig. 1; $R = 100$ nm

Substituting expressions (23) and (24) into Eq. (20) and calculating the remaining projection integrals, we obtain the propagation equation for the slowly varying amplitude $\psi(z)$:

$$i\partial_z\psi + i\Lambda\psi + \Upsilon|\psi|^2\psi = 0, \tag{25}$$

where $\Upsilon = g\gamma, \Lambda = \sqrt{g}\alpha$ and

$$\alpha = \frac{\pi}{\beta P}\int_0^{+\infty}\rho\epsilon_b|\vec{e}|^2 d\rho, \tag{26}$$

$$\gamma = \frac{4\pi k^2}{3\beta^2 P^2}\int_0^{+\infty}\rho\epsilon_a n_2\left[|\vec{e}|^4 + \frac{1}{2}|\vec{e}^2|^2\right]d\rho. \tag{27}$$
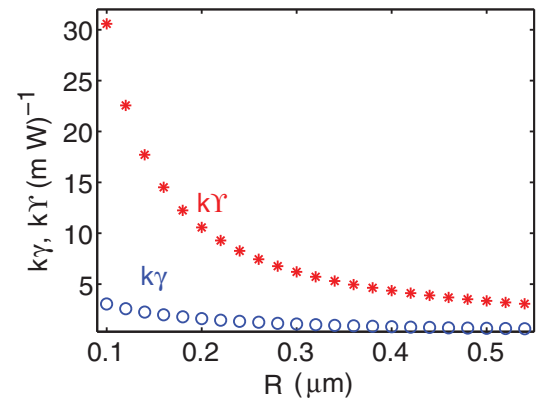

FIG. 3. (Color online) Nonlinear coefficients of the silver waveguide mode as in Fig. 1 as functions of the waveguide radius; $\lambda = 500$ nm.
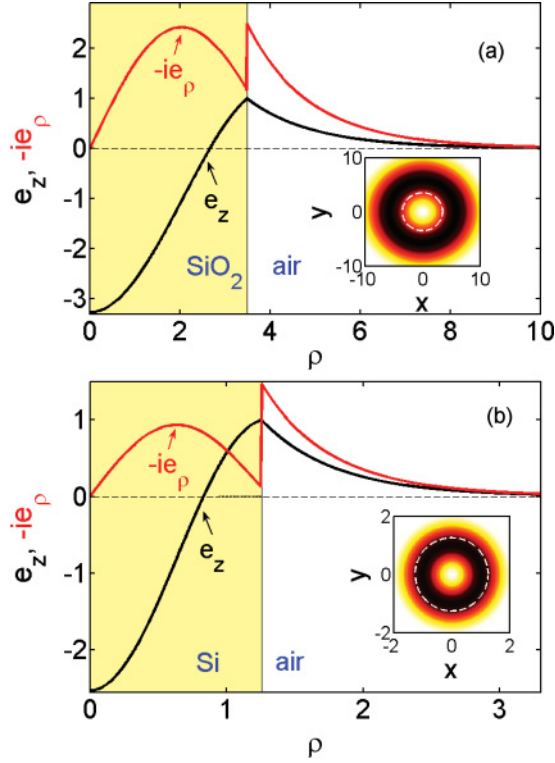
FIG. 4. (Color online) TM guided modes, $m = 0$, of silica glass (a) and silicon (b) rod waveguide with air cladding, $R = 300$ nm, $\lambda = 540$ nm in (a), $R = 600$ nm, $\lambda = 3$ μm in (b). Insets show the cross sections of the z component of the Poynting vector; colors change from black corresponding to large positive values to white corresponding to zero. Waveguide interface is indicated with the dashed white line.

Here, we used $\chi_3 = (4/3)n_2\epsilon_0 c\epsilon_a$, where n_2 is the Kerr coefficient. Parameter γ is defined in the spirit of approaches dating back to the use of the scalar wave equation [8]. Importantly, the nonlinear coefficient Υ differs from γ by the *surface-induced enhancement factor* g:

$$g = 1/(1 + \eta)^2, \qquad (28)$$

where η is provided by Eq. (15). The square root of the same factor is responsible for enhancement of the loss coefficient Λ.

As seen from Eq. (15), the enhancement factor is determined by the product of the amplitude of longitudinal component e_z and the jump in amplitude of the radial component e_ρ at the waveguide interface. For convenience, in the examples below we scale the linear modes in such a way that $e_z(\rho = r) = 1$.

The units of n_2 are m^{2}W^{-1} and the units of γ, Υ are W^{-1}. If one considers the dimensional longitudinal coordinate $Z = z/k$ instead of the dimensionless z, the resulting nonlinear coefficient is $k\Upsilon$, which is measured in m^{-1}W^{-1}. Neglecting the surface contribution η, the expression for the nonlinear parameter is equivalent to the one achieved with traditional methods [8,14,15].

It is worthwhile to clarify how our results relate to the approach based on the reciprocity theorem [6,10,16]. Equation (13) can be transformed to $P = (1 +$
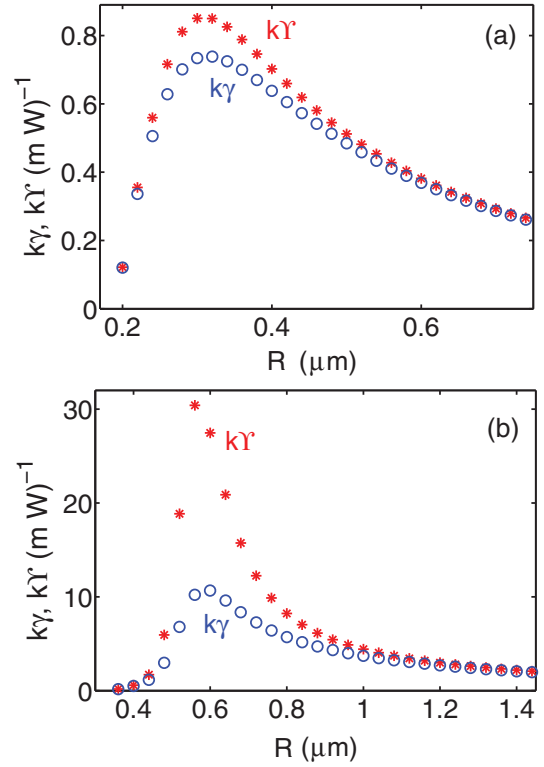

FIG. 5. (Color online) Nonlinear coefficients for the dielectric waveguide modes as in Figs. 4(a) and 4(b), respectively, as functions of the waveguide radius. $\lambda = 540$ nm in (a) and $\lambda = 3$ μm in (b).

$\eta)^{-1} \int \int \rho \text{Re}[\vec{e} \times \vec{h}^*] \cdot \hat{z} d\rho d\phi$, where $\hat{z}$ is the z-direction unit vector and the integration is performed across the entire waveguide cross section. Thus, the nonlinear parameter Υ can be expressed as

$$\Upsilon = \frac{k^2}{3\beta^2} \frac{\int \int \rho \epsilon_a n_2 [2|\vec{e}|^4 + |\vec{e}^2|^2] d\rho d\phi}{\left(\int \int \rho \text{Re}[\vec{e} \times \vec{h}^*] \cdot \hat{z} d\rho d\phi\right)^2}, \qquad (29)$$

which coincides with the expression for the nonlinear coefficient reported in Refs. [6,10,16].
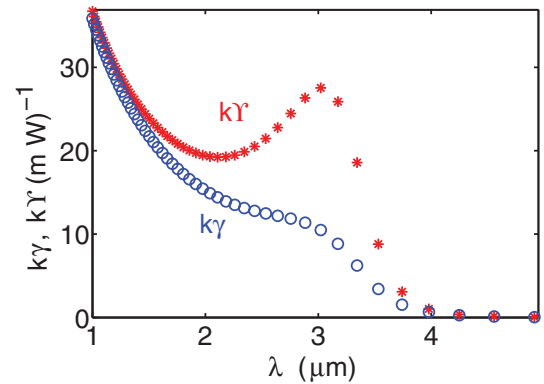

FIG. 6. (Color online) The same as Fig. 5(b) but as functions of the wavelength for the fixed radius $R = 600$ nm. The resonant enhancement of nonlinearity is observed near $\lambda_0 = R\sqrt{\epsilon_I}/0.7 \approx 3$ μm.
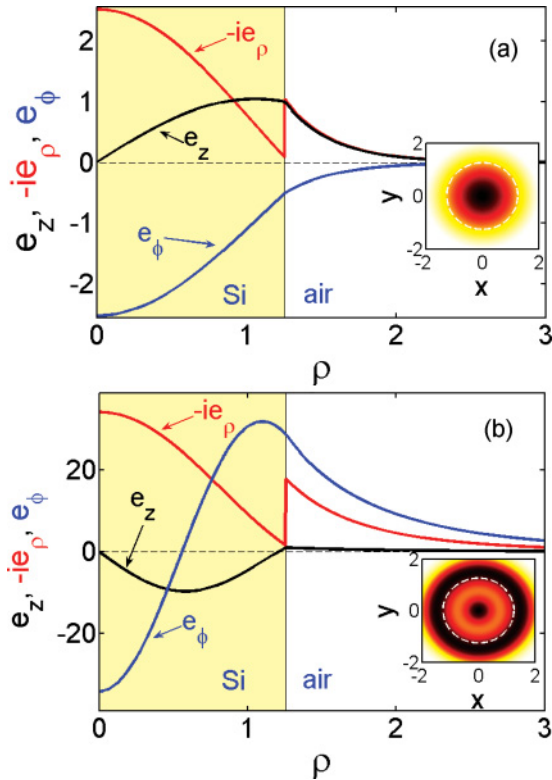
FIG. 7. (Color online) The same as Fig. 4 but for $m = 1$ modes of the silicon waveguide: HE_{11} mode (a) and EH_{11} mode (b).

FIG. 8. (Color online) The same as Fig. 5 but for $m = 1$ modes as in Figs. 7(a) and 7(b), respectively.

V. EXAMPLES

In this section, we identify the surface-induced contributions to the effective loss and nonlinearity parameters Λ and Υ for different waveguide materials and geometries.

A. Plasmonic waveguide

First, we consider a silver rod waveguide surrounded by silica glass. Silver was treated as a purely linear material, while silica glass gives a nonlinear contribution to the displacement vector. We model the metal susceptibility $\epsilon_I(\omega)$ by the Drude-Lorentz fit of the experimental data [17], and the silica glass susceptibility $\epsilon_O(\omega)$ by the Sellmeier expansion [8]. The nonlinear Kerr coefficient of silica glass is fixed to $n_2 = 3 \times 10^{-20} \mathrm{m}^2/\mathrm{W}$.

Figures 1–3 summarize the results for the $m = 0$ guided mode; we found modes with $|m| > 0$ to exhibit similar behavior. For the case of plasmonic waveguide, only TM guided modes are allowed with nonzero e_z and e_ρ components. Both electric field components have peak amplitudes at the waveguide interface, and the discontinuity in e_ρ is well pronounced due to ϵ_I and ϵ_O being of opposite signs (see Fig. 1). We have found that the phase relation between e_z and e_ρ is always such that the surface coefficient η in Eq. (15) is negative: $-1 < \eta < 0$. This results in the surface-induced enhancement of nonlinearity and loss: $g > 1$; see Eq. (28). In Figs. 2(a) and 2(b) we compare the corresponding coefficients computed through the conventional scalar wave approach [8] (γ, α) and given by our theory (Υ, Λ) as functions of the wavelength for a fixed waveguide radius. The discrepancy
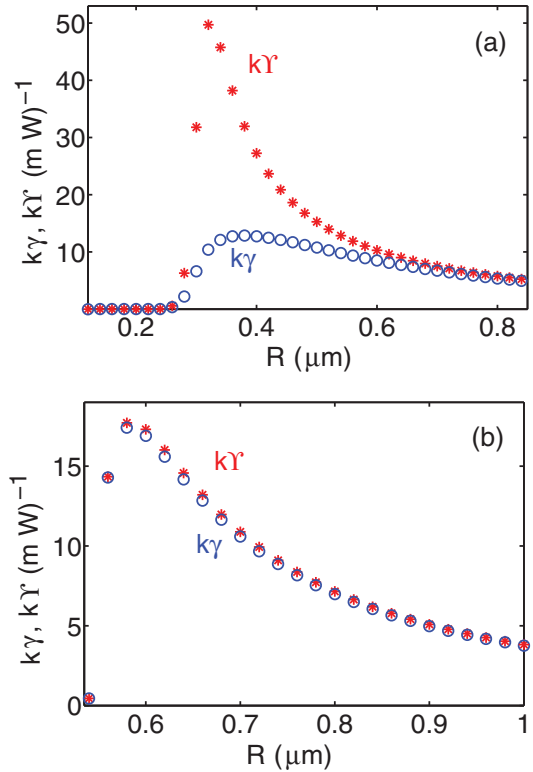
between the two theories becomes significant as wavelength decreases. Approaching the surface plasmon resonance $\lambda = \lambda_{\mathrm{SPP}} \approx 370$ nm $[|\epsilon_I(\lambda_{\mathrm{SPP}})| = \epsilon_O(\lambda_{\mathrm{SPP}})$ [3]], the mode is getting tightly localized at the interface, and the enhancement factor g tends to infinity.

Resonant enhancement of the nonlinear response near the plasmonic resonance can also be found in the context of nanoparticles (see, e.g., Refs. [18–20]).

For a fixed wavelength, the surface-induced enhancement factor grows as the waveguide radius decreases (see Fig. 3). Earlier we reported similar behavior for the metal slot planar geometry [9]. Note, there is no cutoff for plasmonic waveguide modes, which gives an opportunity to tune the effective nonlinear parameter to virtually any high value (although, at the cost of the enhanced loss).

In order to validate our theory, we calculate the loss parameter of the modes directly via the dispersion relation in Eq. (12). By substituting the complex-valued ϵ_I of metal directly in Eq. (12), we obtain the corresponding complex-valued propagation constant $\beta = \beta_r + i\beta_i$. The imaginary part β_i gives the decay rate of the corresponding mode, and is plotted in Fig. 2(b) with the solid curve. It perfectly agrees with the effective loss parameter Λ calculated with the help of our perturbation theory.

B. Dielectric waveguide

Next, we consider a dielectric rod waveguide with an air cladding ($\epsilon_O = 1$). Figures 4–5 summarize our analysis of the TM modes of silica glass and silicon waveguides. For the latter we modeled dielectric susceptibility $\epsilon_I(\omega)$ with the help

of the Herzberger expansion [21], while the Kerr coefficient was fixed to $n_2 = 4.5 \times 10^{-18} \text{m}^2/\text{W}$.

Similar to the above case of a plasmonic waveguide, TM modes of the dielectric waveguides have a nonzero e_ρ component with discontinuity at the waveguide interface (see Fig. 4), ensuring a nonzero surface contribution to the effective nonlinearity coefficient. For the case of a silica glass waveguide, the refractive index contrast $|\epsilon_I - \epsilon_O|$ is relatively weak ($\epsilon_I \sim 2$). As a result, the surface contribution remains relatively small throughout a wide range of waveguide radius and wavelengths. In Fig. 5(a) nonlinear coefficients are plotted as functions of the waveguide radius at the fixed wavelength $\lambda = 540$ nm. The maximum discrepancy between the coefficients γ and Υ is observed at a certain waveguide radius $R_0 \sim 300$ nm, where the nonlinearity is boosted by about 15% via the surface effects ($g \sim 1.15$). The use of traditional perturbative theories is justified for such waveguides with low refractive index contrast.

Replacing silica glass with silicon [4–7], the refractive index contrast is considerably raised ($\epsilon_I \sim 12$ for silicon) and the mode becomes more localized [cf. insets in Figs. 4(a) and 4(b)], altogether leading to much higher values of the surface-induced enhancement factor g. Fixing the wavelength at $\lambda = 3$ μm, we observe massive enhancement of nonlinearity by about 200% for the waveguide radius $R_0 \sim 600$ nm, where $g \sim 3$ [see Fig. 5(b)].

While in plasmonic waveguides the nonlinearity enhancement is greatly pronounced near the plasmonic resonance (i.e., at a certain wavelength which is determined by the *material* properties of the waveguide), in dielectric waveguides we deal with the *geometrical* type of resonance. At any fixed wavelength, the difference between γ and Υ reaches its maximum at a certain waveguide radius R_0, while it becomes negligible away from the resonance (see Fig. 5). We found that for $m = 0$ modes the resonance condition can be approximated by the linear relation between the waveguide radius and the wavelength inside the dielectric core: $R_0 \sim 0.7\lambda/\sqrt{\epsilon_I}$. We confirmed this observation by considering dependencies $\gamma(\lambda)$ and $\Upsilon(\lambda)$ for a fixed waveguide radius (see Fig. 6).

Similar resonant enhancement of nonlinearity is observed for modes with $m \neq 0$. In Fig. 7 the profiles of HE_{11} (which is the fundamental mode) and EH_{11} modes of the silicon waveguide are shown. The corresponding nonlinear coefficients as functions of the waveguide radius are plotted in Fig. 8. The surface effect is much stronger for the HE_{11} mode, since this mode has stronger e_ρ and e_z components and is more localized than the EH_{11} mode [cf. Figs. 7(a) and 7(b)]. The resonant enhancement of nonlinearity for $m = 1$ modes happens at a smaller radius (for the fixed wavelength), than for $m = 0$ modes (see Fig. 8).

VI. SUMMARY

A perturbative theory for modeling of nonlinear propagation in rod waveguides with a subwavelength core radius has been developed. In our approach, corrections to boundary conditions due to nonlinearity and loss are rigorously taken into account, which has enabled us to elicit the role of surface effects in enhancement of nonlinearity. The difference between the perturbation theory, based on the scalar wave equations, and our theory is expressed by the unique surface-induced enhancement factor g, Eq. (28), which is determined explicitly by the field discontinuities at the waveguide interface.

The surface-induced enhancement of nonlinearity becomes significant in the regimes of subwavelength guidance, which is illustrated by several examples. In the case of plasmonic waveguides, the enhancement factor g reaches extremely high values near the plasmonic resonance and for small waveguide cores. For dielectric waveguides, g is maximized for certain relations between waveguide radius and wavelength, which are unique for different guided modes. The surface contribution remains small for waveguides with low refractive index contrast (such as silica glass waveguides), but becomes significant when the refractive index contrast is large. The latter particularly applies to semiconductor waveguides (such as silicon nanowires), which are considered as promising candidates for subwavelength light guidance.

[1] E. Ozbay, Science **311**, 189 (2006).

[2] T. W. Ebbesen, C. Genet, and S. I. Bozhevolnyi, Phys. Today **61**, 44 (2008).

[3] A. Boardman, *Electromagnetic Surface Modes* (John Wiley & Sons, New York, 1982).

[4] M. A. Foster, A. C. Turner, J. E. Sharping, B. S. Schmidt, M. Lipson, and A. L. Gaeta, Nature (London) **441**, 960 (2006).

[5] Q. Lin, O. J. Painter, and G. P. Agrawal, Opt. Express **15**, 16604 (2007).

[6] R. M. Osgood Jr., N. C. Panoiu, J. I. Dadap, X. Liu, X. Chen, I.-W. Hsieh, E. Dulkeith, W. M. Green, and Y. A. Vlasov, Adv. Opt. Photon. **1**, 162 (2009).

[7] S. V. Afshar, W. Q. Zhang, H. Ebendorff-Heidepriem, and T. M. Monro, Opt. Lett. **34**, 3577 (2009).

[8] G. P. Agrawal, *Nonlinear Fiber Optics* (Academic Press, San Diego, 2001).

[9] D. V. Skryabin, A. V. Gorbach, and A. Marini, J. Opt. Soc. Am. B **28**, 109 (2011).

[10] S. V. Afshar and T. M. Monro, Opt. Express **17**, 2298 (2009).

[11] D. Marcuse, *Light Transmission Optics* (Van Nostrand Reinhold, New York, 1982).

[12] J. Stratton, *Electromagnetic Theory* (McGraw-Hill, New York, 1941).

[13] J. Takahara, S. Yamagishi, H. Taki, A. Morimoto, and T. Kobayashi, Opt. Lett. **22**, 475 (1997).

[14] A. R. Davoyan, I. V. Shadrivov, and Y. S. Kivshar, Opt. Express **17**, 21732 (2009).

[15] E. Feigenbaum and M. Orenstein, Opt. Lett. **32**, 674 (2007).

[16] F. Ye, D. Mihalache, B. Hu, and N. C. Panoiu, Phys. Rev. Lett. **104**, 106802 (2010).

[17] B. Ung and Y. Sheng, Opt. Express **15**, 1182 (2007).

[18] F. Hache, D. Ricard, and C. Flytzanis, J. Opt. Soc. Am. B **3**, 1647 (1986).

[19] L. Fu and L. Resca, Phys. Rev. B **56**, 10963 (1997).

[20] G. Y. Panasyuk, J. C. Schotland, and V. A. Markel, Phys. Rev. Lett. **100**, 047402 (2008).

[21] D. F. Edwards and E. Ochoa, Appl. Opt. **19**, 4130 (1980).